Biophysically Realistic Modeling of Neuronal Networks: Investigating High-Frequency Oscillations

Anna Villalobos

BSc. Assignment ATLAS
Supervisors: Dr. H.G.E. Meijer and Dr. J.A. Álvarez Chávez

ABSTRACT

High Frenquency Oscillations (HFOs), with a frequency above 80Hz have been proposed as a potential biomarker for the identification of epileptogenic zones in the brain. This is necessary to be able to identify the area that will be resected on medically-refractory patients during surgery. Previous models, such as Morris-Lecar (ML) simulate neuronal behaviour and HFOs. Nevertheless, the morphology of the neuron has not yet been included. The project extends the simulation incorporating neuronal morphology in order to be able to explore its role in neuronal network dynamics. The results are obtained by placing the gap junctions at the soma, dendrite, or axon respectively, and modifying coupling strength to identify its effects. Findings indicate that the addition of compartments significantly impacts the long-term behaviour of the neuronal network.

Keywords: HFOs, Morris-Lecar, multi-compartment neuronal model, epilepsy

1 INTRODUCTION

Epilepsy is a chronic brain disorder that affects around 70 million people globally and it is characterized by recurrent seizures (Cai et al., 2021). Epileptic seizures are episodes of involuntary movement involving part or all of the body. Sometimes they come together with a loss of consciousness and loss of control over bodily functions. These effects are a clinical manifestation of abnormal electrical discharge in the neurons. Nowadays, several different treatments exist, with anticonvulsant medication as the main strategy (NHS, 2020). Unfortunately, these treatments are effective in taking control of the seizures for around two-thirds of the cases. For patients that are medically refractory, surgery can be considered. During an epilepsy surgery the area of the brain involved in the creation of seizures is resected (Cai et al., 2021). Thus, to be able to conduct surgery, it is necessary to identify the areas of the brain related to seizure generation, the epileptogenic and the seizure onset areas. High Frequency Oscillations (HFOs), which are oscillations of a frequency above 80Hz, have been proposed as an electrophysiological biomarker for these areas of the brain. HFOs can be observed in electroencephalography (EEG) during the occurrence of spontaneous seizures, where the electrical impulses of the brain are recorded. Nevertheless, this can only be done to patients that have already been diagnosed, since intracranial EEG is used. Due to the invasive nature of the procedures involved it is not ethical for a control group

to undergo this medical experiment. For HFOs, the voltage from action potentials is recorded.

Action potentials are rapid sequences of changes in the voltage across the neuronal membrane that allow neurons to transmit electrical signals (van Putten, 2020). The process the cell undergoes throughout an action potential is the following. First, the cell is found at a resting state (−70mV). When a stimulus reaches the neuron, the ion channels open, allowing the flow of Na^+ and K^+ ions. This causes the membrane potential to depolarize. If the potential reaches a critical level, then an action potential is triggered. This usually happens around −55mV. Once this state is reached, more ion channels open which cause a rapid increase on membrane potential until it returns to rest.

Neurons are the main component of the central and peripheral nervous systems. They are essential for our bodies to be able to process and transmit information (Caire et al., 2020). They are composed by the soma or cell body, that contains the nucleus, the dendrites, and the axon (see Figure 1). The dendrites receive the information from other neurons which is then transported to the soma. In the soma, the information is processed and a response is sent through the axon to other neurons. Neuronal morphology is the most complex out of all the human cells. Being able to understand neuronal morphology and its impact on neuronal network dynamics is one of the current focuses of neuroscience (Gowers and Schreiber, 2024).

The reason of this captivation towards neuron morphology emerges from the influence it has in their function and interaction within networks. The behaviour of neuronal networks can be modeled regarding the cell membrane as an electrical circuit. Hodgkin and Huxley (1952) provided insights into the electrical characteristics of neurons. Their work was a milestone towards understanding how action potentials are generated and propagated. Nevertheless, it simplifies the neuron to just a point (soma), excluding other compartments like the dendrites and axons.

Nowadays, computational scientists aim to make these models more biophysically re-

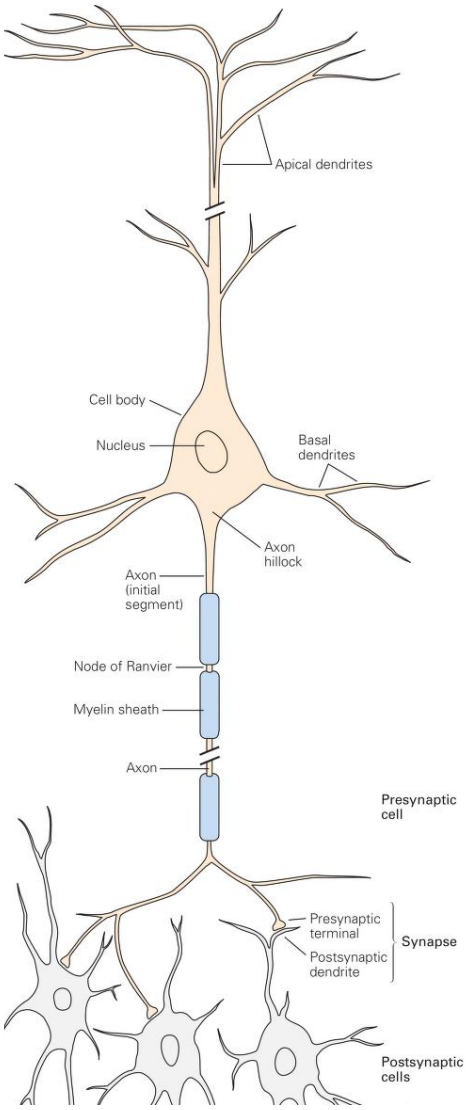

Figure 1. Schematic of a neuron with an axon and a dendritic tree (Kandel et al., 2013).

alistic, by including the spatial complexity of
neurons (van Pelt et al., 2001). Another often used 2D model is the Morris-Lecar mode (Morris and Lecar, 1981), it describes the oscillatory behaviour of neurons, which is essential for understanding neurological events, such as HFOs.

This research integrates biophysically realistic neuronal structures to the Morris-Lecar model (Morris and Lecar, 1981). Using the same parameters as Přibylová et al. (2024) to obtain UFOs. To incorporate the dendrite and axon we use the stick-and-ball model, which regards the dendrite and axon just as two sticks (see Figure 2). Then, gap junctions are placed at the soma, dendrite, and axon. For the results, the effects of placing the gap junctions at different compartments on Anti-phase behaviour is researched.

Figure 2.
Representation of the stick-and-ball model of one neuron.

This research could make contributions to both scientific knowledge and human health, since it connects basic science and its clinical applications.

2 CONTEXTUAL EXPLORATION

This project focuses on the simulation of High Frequency Oscillations in biophysically realistic models. Even though this topic is fairly specific, its results could have greater contributions. Its broader relevance is related to the fields of neuroscience, computational modelling and health sciences.

As mentioned before, HFOs have been proposed as an electrophysiological biomarker for the epileptogenic zone (EZ). For epileptic patients that need epilepsy surgery it is crucial to be able to identify this area, since this is the part of the brain that is resected during the medical procedure. The resection of the EZ should stop the emergence of seizures since it is the area where seizures emerge (Cai et al., 2021). This requires open brain surgery, which is already on itself a challenge. Furthermore, while resecting part of the brain, it is crucial that none of the areas that control important brain functions like speech, movement, memory or vision are affected. In most cases, these functions are performed by different parts of the brain, but the team assessing the case should take into account. Therefore, it is also important that the surgical team resects as little of the brain as possible, while, of course, still resecting all the necessary area (Panzica et al., 2013). Precise identification of the EZ is a challenge every time. Removal of brain tissue that generates HFOs has been linked to better post-surgical outcomes than removal of the seizure onset zone (Zijlmans et al., 2012).

HFOs have also been associated with other disorders and diseases. For example, in Parkinson's disease, oscillations by stimulation in the range of $250-500$Hz in the basal ganglia may influence the effectiveness of Deep Brain Simulation treatments (DBS) (Brown, 2003). Furthermore, cognitive decline is associated with abnormal oscillations in the gamma range ($30-80$Hz). And changes on those oscillations have also been associated with Alzheimer (Tülay et al., 2020).

This project executes the simulation of two neurons communicating with each other through gap junction coupling. This is relevant to the field of computational

neuroscience since the simulation includes morphological aspects of the neuron. The Morris-Lecar model has been used in previous works for the modelling of High Frequency Oscillations. Přibylová et al. (2024) used gap junctions on the soma to create higher frequencies. The neuron was regarded as a point-neuron, considering only the cell body. Adding dendrites and axons to this model, even if it is only using the stick-and-ball model, could improve the accuracy of the model, and give different results. This is of course applicable to this specific model, but could also be applied to other simulations of neuronal networks. It has been proven that neuronal morphology has an impact on signal propagation dynamics (Ofer et al., 2017). Therefore being able to have more biophysically realistic models of neurons will help to accurately model neuronal connections.

Computational neuronal models are a tool to simulate known models, like the Morris-Lecar model. But they could additionally be a tool to improve our understanding on the brain's activity and organisation (Ofer et al., 2017). Furthermore the exploration of these models could help answer fundamental neuroscience questions and obtain knowledge for practical uses in medicine, such as for epilepsy surgery, as mentioned above.

This thesis also dives into the (a)synchronisation of neuronal networks. As mentioned before, the morphology can affect signal propagation and impact the spiking of a neuron. Gowers and Schreiber (2024) demonstrate that dendritic arborization switches the neuron's spiking type. Morphology can even impact the network's behaviour to induce either synchronous or asynchronous behaviour. With the model that has been used for this thesis, both in-phase and anti-phase behaviour can be observed. Furthermore, the results study how the Anti-Phase behaviour is destroyed when the gap junctions are added to different compartments.

Limitations

The extent to which HFOs can be used to identify the resected area is however still unknown, and thus further research still needs to be conducted. Most of this research needs to be done without a control group, since the medical procedures involved in observing HFOs, are highly invasive and involve intracranial procedures. For this reason, it cannot yet be affirmed that HFOs are a biomarker for epilepsy (Zijlmans et al., 2012). A trial has proved that HFOs to tailor epilepsy surgery is not non-inferior than spike- guided tailoring (Zweiphenning et al., 2022). They have been recorded in drug-resistant patients, and the resection of the area producing these oscillation has demonstrated a better outcome than the resection of the seizure-on-set area, thus validating the clinical relevance of the HFO area in the individual patient with an automated procedure (Fedele et al., 2017). Nevertheless, the occurrence of HFOs in non-epileptic patients is unknown. HFOs can also not be used for the diagnostic of epilepsy, due to the aforementioned invasive medical procedures. Nowadays, the identification of HFOs and the area where they are generated is done after an epilepsy diagnosis. The development of new non-invasive medical procedures could help in understanding further the presence and effect of HFOs.

3 LITERATURE REVIEW

3.1 High Frequency Oscillations

High Frequency Oscillations (HFOs) are patterns of electrical activity in the brain characterized for having an elevated frequency in comparison to typical neuronal oscillations ($1-150$Hz). HFOs can be divided into different types, like interictal high gamma ($65-100$Hz), ripples ($100-250$Hz), fast ripples ($350-600$Hz), very high-frequency oscillations (VHFOs, $600-2000$Hz), very fast ripples (VFRs, $600-1000$Hz), ultra-fast ripples (UFRs, $1000-2000$Hz) and ultra-fast oscillations (UFOs, over 2000Hz). HFOs can either be physiological, present in normal conditions of the brain, or pathological, which are then associated with disorders (Jefferys et al., 2012).

These oscillations can be generated through several complex mechanisms that involve both intrinsic properties of the neurons and synaptic interactions in neuronal networks. It is believed that they can be generated through the synchronization of neuronal activity in the brain, specially if it is originated in the regions that are associated to epilepsy (epileptogenic zone, and seizure onset zone) (Engel and da Silva, 2012). Usually, these oscillations are related to abnormal patterns of neuronal spikes, and are observed in patients with epilepsy, specially in drug-resistant patients (Brázdil et al., 2023). Přibylová et al. (2024) suggest that weak gap junction coupling in epileptic regions High Frequency Oscillations could be produced.

3.1.1 HFOs in the Context of Epilepsy

In the context of epilepsy, HFOs have been identified as potential biomarkers for epileptogenic zones in the brain, which makes them an area of interest for the investigation and treatment of this neurological disorder (Cai et al., 2021). The reasoning behind this is that they may be indicative of areas where seizures are originated. The presence of HFOs in electroencephalograms (EEGs) has been associated with ictal activity and the resection of cerebral areas that exhibit HFOs has been shown to improve the results of surgery in patients with epilepsy. The creation of new simulation models enables scientists to test hypotheses and to get a better understanding of the workings of these mechanisms.

3.2 Synchronization of Neuronal Networks

Phase synchronization in neuronal networks has an important function for brain functions such as memory, learning, and perception (Kazemi and Jamali, 2022). Furthermore, it is considered essential for information processing in the nervous system (van Wijk et al., 2012)

Neuronal networks coordinate through synchronization and that is how collective neuronal behaviours arise.

Kazemi and Jamali (2022) propose that neuronal synchronization plays a role in the pathophysiology[1] of epilepsy, which could lead to seizure activity. Studying the underlying processes of network synchronization could also improve the understanding of epilepsy. Additionally, with more biophysically realistic neuronal simulations the

[1] Physiological processes associated with a disease or injury

results obtained on synchronization could differ from the ones obtained using a point-neuron.

In epileptic patients, during seizures there is an excessive synchronization of large neuronal populations. Studies of *in vivo* and *in vitro* models of epilepsy and seizures revealed synchronous firing in microdomains (Jiruska et al., 2013). This was present during epileptogenesis and ictogenesis, and was manifested in extracellular recordings as high frequency signals (Bragin et al., 2000).

After the start of a seizure, Cymerblit-Sabba and Schiller (2012) observed the appearance of desynchronization in local field potentials and neural activity. Additionally, Jefferys et al. (2012) demonstrated that spatial scale has an impact on synchronization in the genesis of interictal pathological HFOs. It has been observed how population of cells can synchronize their action potential firing (Foffani et al., 2007). This is manifested as HFOs in local field potentials. In a chronic epileptic brain, fast ripples up to 800Hz have been recorded (Bragin et al., 2000).

Towards the end of a seizure synchronization reaches its peak. It has been observed how seizures terminate at different areas of the brain at the same time. Thus, disrupting or enhancing synchronization might be able to promote seizure termination, and therefore be used as abortive therapy (Foffani et al., 2007).

3.3 Morphology of the Neuron

Neurons, together with glial cells, are the cells that are part of the central and peripheral nervous systems. Through these systems, animals can communicate to the external environment, receive signals, processing information, and emitting responses. Neurons carry out these functions since they are specialized in the reception, processing, and projection of information through chemical and electrical mechanisms.

The morphology of neurons is the most complex out of all the cells in the human body. Neurons are divided into the soma, dendrites and axon. The soma or cell body is the main part of the neuron, and it contains many organelles including the cell nucleus (Caire et al., 2020). At the soma most of the neurotransmitters are synthesized and then transported to the end terminals of the axon for synapses. Dendrites are the part of the neuron that has a receptive function in the physiology of the neuron. They relay signals that come in from other neurons to the cell body, where they are combined and then trigger a response. The axon is a cable emerging from the cell that conducts action potentials (electrical impulses) away from the nerve cell body.

3.4 Existing Simulation Models

Existing models have shown promise in generating UFOs in small neuronal networks with gap junction coupling, but have ignored spatial properties. Gap junctions are typically placed in a model on the soma rather than axons or dendrites, and all-to-all coupling is often assumed, neglecting the impact of realistic connectivity patterns.

Previous research has proven that neuronal morphology impacts the synchronization state of neuronal networks (Gowers and Schreiber, 2024). Changes in the size of dendritic trees could alter the behaviour of the networks, going from an anti-phase behaviour to in-phase. This suggests that neuronal morphology can affect how susceptible neuronal tissue is to synchronization. In-phase activity means that the neurons

are spiking at the same time, and therefore, their oscillations are in-phase.

3.5 Research Question

To address these limitations, this thesis proposes to create a more biophysically realistic neuronal network model with gap junction coupling. Specifically, the project focuses on exploring the effect of adding dendrites and axons to the model, with additional compartments to capture the spatial complexity of neuronal morphology. After the creation of the simulation, the objective is to see how gap junctions placed at the soma or axons would destroy anti-phase behaviour.

4 METHODS AND MODELS

In this section, we describe the models used. First, an explanation of the Hodgkin-Huxley model is given, followed by an explanation of the Morris-Lecar model. Then we mention how we add dendrites and axons, as well as gap junctions.

4.1 Hodgkin and Huxley Model

The Hodgkin-Huxley model describes the characteristics of a cell membrane as an electrical circuit. In this case the semipermeable cell membrane acts as the capacitor. Therefore, once an input $I(t)$ is injected into the system, it can either add an additional charge to the capacitor or leak through the channels of the membrane. A channel has a leak resistance R, R_{Na} for the sodium channel and R_K for the potassium one. The latter two are not fixed values but change with the opening or closing of the ion channel gates (see the functioning in Figure 3).

The Nernst or Reversal potential is the membrane potential at which an ion is in equilibrium. An example of a Nernst potential for an ion of potassium (K^+) is calculated the following way:

$$E_{K^+} = -\frac{RT}{zF} ln\left(\frac{[K^+]_{in}}{[K^+]_{out}}\right), \tag{1}$$

where R is the gas constant, T the absolute temperature in Kelvin, z the valence, and F is Faraday's constant. The Nernst potential is different for each ion, thus, to be able to calculate the equilibrium we have to compute the weighted average between all ions. In the Hodgkin-Huxley model, the Nernst potential which is generated by the difference in ion concentration is represented by a battery (Gernster et al., 2014).

Since we can consider this model to be an electrical circuit, according to the conservation of electric charge on a membrane segment, the applied current $I(t)$ can be split into a capacitive current I_C, which charges the capacitor C, and additional components I_i defined by the ion currents.

$$I(t) = I_C(t) + \sum_i I_i(t) \tag{2}$$

In the original model described by Hodgkin-Huxley, three types of channels were described: a sodium channel (Na), a potassium (K) and a leak channel. Hence, from the definition of capacity $C = q/u$, and the previous equation (2), we obtain:

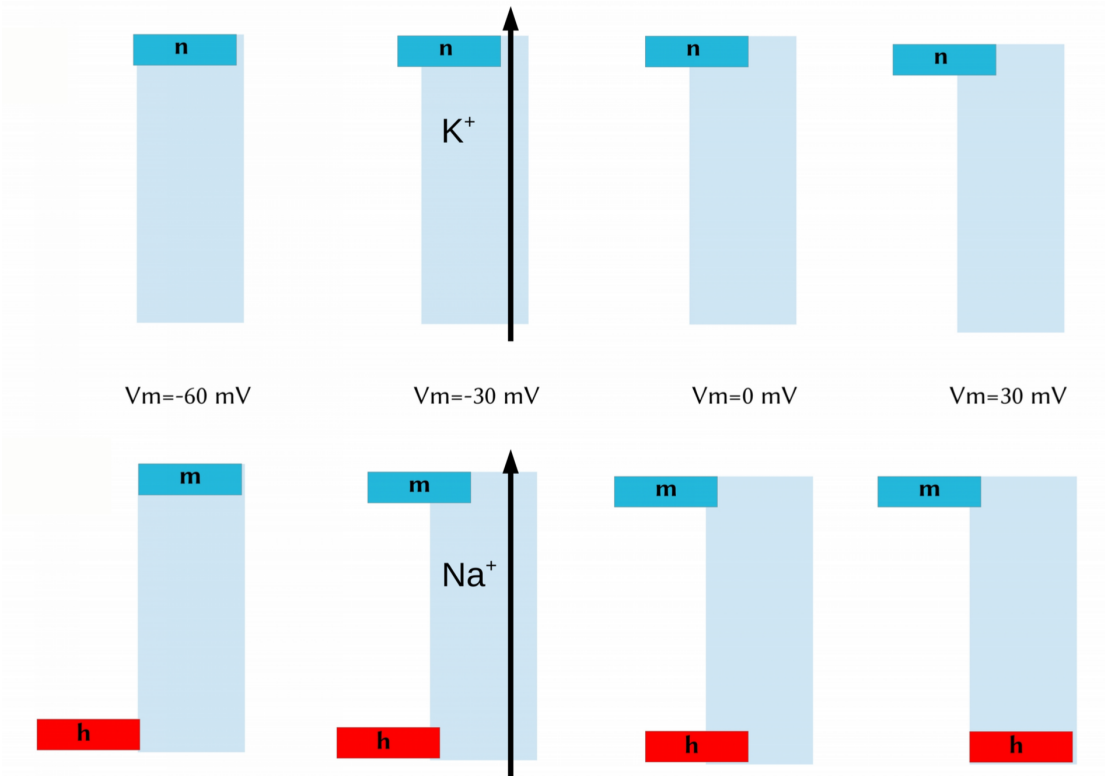

Figure 3. Opening and closing of single and double gates for potassium and sodium ions, n represents the ion gate for potassium, and m and h the ones for sodium (van Putten, 2020).

$$C\frac{dV}{dt} = -\sum_i I_k(t) + I(t) \tag{3}$$

where V stands for the voltage across the membrane and $\sum_k I_k$ is the sum of all ionic currents that go through the cell membrane.

In this case, we are only considering the previously mentioned sodium and potassium channels. Thus, the membrane voltage V can be calculated using the following equation, taking into account the current from both ions:

$$C\dot{V} = I - I_{Na} - I_K + I_{Leak} \tag{4}$$

Each ionic current is equal to the product of their conductance and the voltage difference. For an unspecified ion i, the equation would look as followings:

$$I_i = g_i(V - E_i) \tag{5}$$

If we substitute all the ionic currents in the equation we obtain Equation 6. The conductances involve ion gates in a nonlinear way, since, as seen in Figure 3 the opening and closing of said gates depends on the membrane potential.

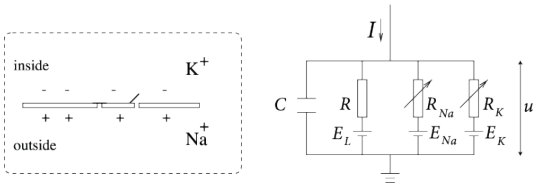

Figure 4. Cell membrane represented as an electrical circuit described by Hodgkin and Huxley model.

$$C\dot{V} = I - g_{Na}(V - E_{Na}) - g_K(V - E_K) - g_L(V - V_L) \tag{6}$$

4.2 Morris-Lecar Model

The Morris-Lecar (ML) model is a mathematical model created in 1981 (Morris and Lecar, 1981). It simulates the oscillatory behaviour of neurons in relation to the conductances of Calcium (Ca^{2+}) and Potassium (K^+) ions. Originally, it mimicked the potential across muscle fibers in a giant barnacle. Later on, its applications were widespread in modelling neurons (Přibylová et al., 2024; Tsumoto et al., 2006). The model consists of a system of two differential equations which describe the behaviour of neuronal networks by modelling membrane potential and gating variable dynamics.

With parameters appropriate to a nerve axon, the model yields prototypical single-shot firing, with a quasi-threshold, and an abrupt transition to repetitive firing over a narrow frequency range. Using parameters appropriate to a weak excitation current, the model displays spike trains emerging from zero frequency and oscillating over a relatively wide range of frequencies. The model is described as follows:

$$\begin{cases} C\dfrac{d}{dt}V = -g_{Ca}m_{inf}(V)(V - V_{Ca}) - g_K w(V - V_K) - g_L(V - V_L) + I_{ext} \\ \dfrac{d}{dt}w = \dfrac{(w_{inf}(V) - w)}{{}_w(V)} \end{cases}, \tag{7}$$

where V is the membrane potential, w is the activation variable for K^+ current, which is the average fraction of open channels. And C $[\mu F]$ is the cell membrane capacitance. The Ca^{2+} current is assumed to activate instantly according to:

$$m_{\text{inf}}(V) = \frac{1}{2}\left[1 + \tanh\left(\frac{V - \beta_1}{\beta_2}\right)\right], \tag{8}$$

β_1 and β_2 are the potential and slope at which the ion's current is half-activated. The voltage-dependent steady state w_{inf} is described the following way:

$$w_{\text{inf}}(V) = \frac{1}{2}\left[1 + \tanh\left(\frac{V - \beta_3}{\beta_4}\right)\right]. \tag{9}$$

Parameters β_3 and β_4 are comparable to β_1 and β_2. The timing scale for the variable w is:

$$\tau_w(V) = \frac{1}{2}\left[\phi \cosh\left(\frac{V-\beta_3}{2\beta_4}\right)\right]^{-1}, \tag{10}$$

where the temperature constant ϕ adjusts the relative timescale of V and w.

The Morris-Lecar equations essentially describe "push-pull" relaxation oscillations, with g_{Ca} and g_K and the corresponding equilibrium potentials V_{Ca} and V_K determining the relative strengths of push to pull. The system can be excitable as the current I_{Ca} provides positive feedback.

By changing parameters $g_{gs}, g_{gd}, g_{ga}, g_{pa}, g_{pd}, g_{ca}, g_{cd}$, the Morris-Lecar equations describe the two main classes of nerve oscillations first described by Hodgkin and Huxley (1952) as well as other types of behaviour. The distinct oscillation classes are seen in Figure 5

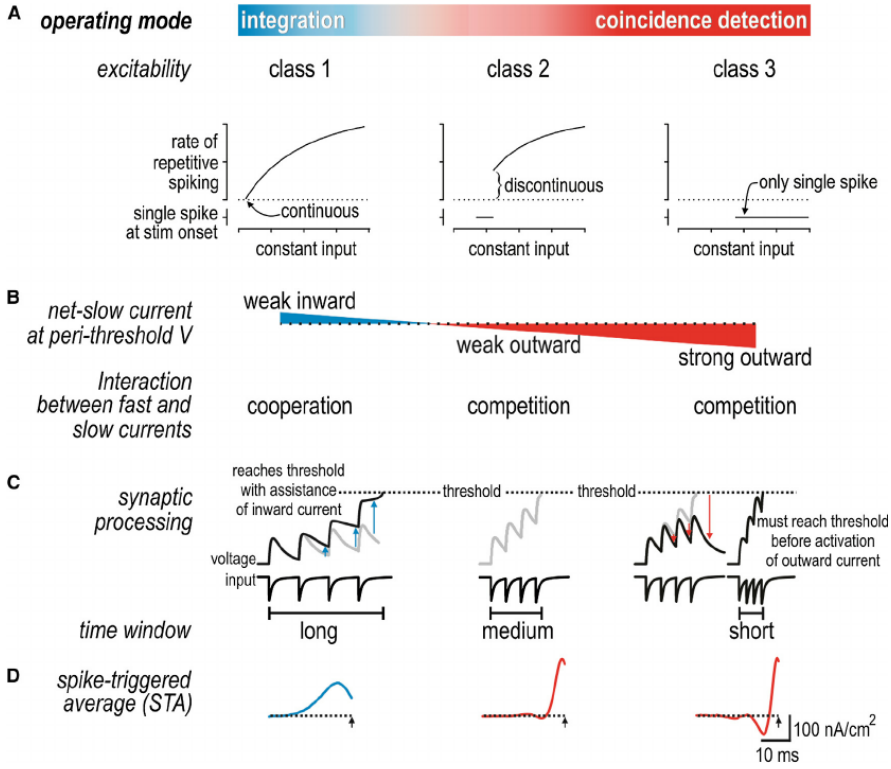

Figure 5. The three types of excitability of neurons described by Hodgkin and Huxley (1952), pictured obtained from Ratté et al. (2013).

4.3 Simulation details

Previously, the morphology of the neuron was described with the intention of making this simulation biophysically more realistic. Nevertheless, it is important to note that some liberties were taken when building the simulation. A neuron can have different shapes depending on its functionality. Therefore, the sizes of the added compartment would differ from one type to another.

In this study, we employ a simplified neuronal geometry, the so-called stick-and-ball model. This simplifies the cell morphology into two 'sticks' (the axon and dendrite) and a ball (the soma).

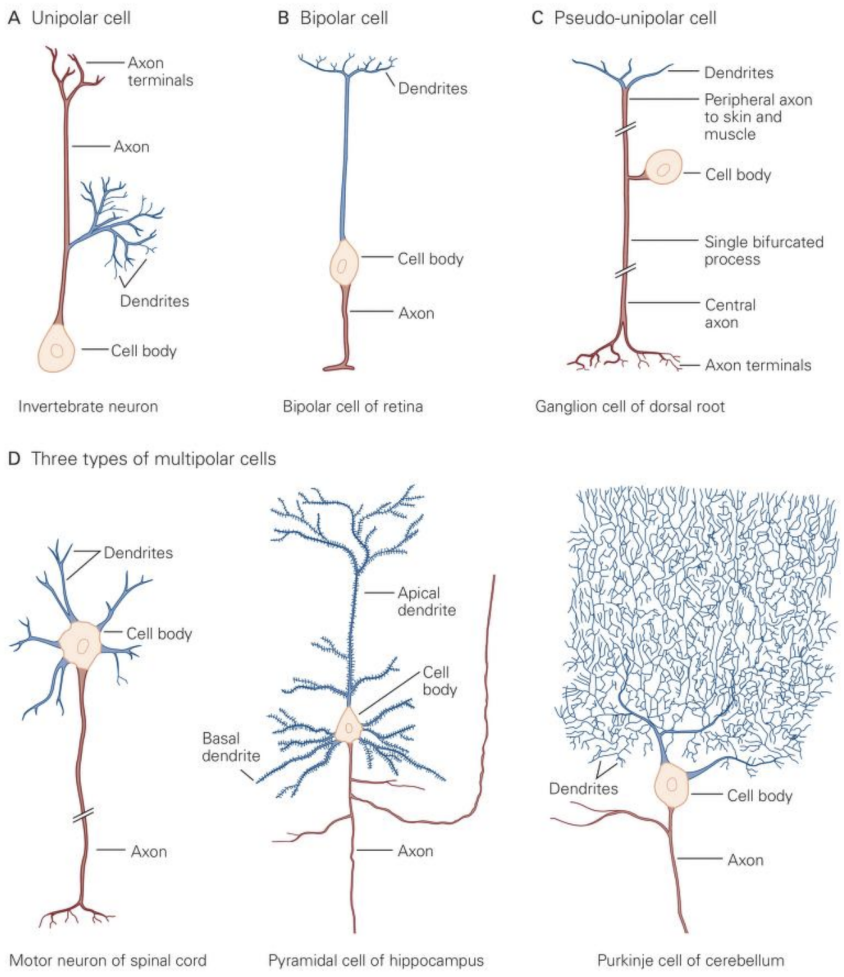

Figure 6. Example of different dendritic trees, picture obtained from Kandel et al. (2013).

To model the neurons, Brian2, a neuron-simulation environment built in Python was used. Gap junction coupling was described using the previously mentioned Morris-Lecar model (Equation 7), based on Přibylová et al. (2024). The parameters used can be found on Table 1.

To test the impact of adding dendrites and axons to the model, two neurons were built with the morphology mentioned above. These neurons communicate with each other through the connections drawn in Figure 7. Additionally, each soma is connected to the axon and dendrites. The relative size of the cell body compared to the other compartments was investigated. The model is able to reproduce both in-phase and anti-phase behaviour of the two neurons. The results are obtained by recording the potentials at the soma, dendrite and axons.

4.3.1 Fitting of the Model

In the model, we focus on the equations described by the Morris-Lecar Model, which describe electrical connections between the neurons. Chemical connections were ignored since for Ultra-Fast Frequency Oscillations it is important that connections

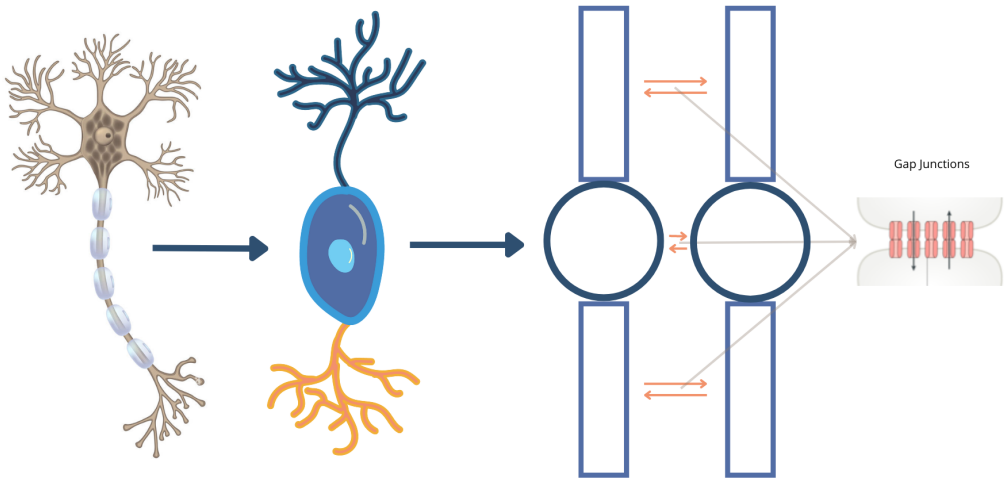

Figure 7. Sketch of the simplification of a neuron used, representing the stick-and-ball model of two neurons (right).

Parameter	Value
g_{Ca}	$4\,\mathrm{mS/cm^2}$
g_K	$8\,\mathrm{mS/cm^2}$
g_L	$2\,\mathrm{mS/cm^2}$
V_{Ca}	$120\,\mathrm{mV}$
V_K	$-80\,\mathrm{mV}$
V_L	$-60\,\mathrm{mV}$
ϕ	$\frac{1}{15.0\,\mathrm{ms}}$

Parameter	Value
β_1	$-1.2\,\mathrm{mV}$
β_2	$18\,\mathrm{mV}$
β_3	$10\,\mathrm{mV}$
β_4	$17.4\,\mathrm{mV}$
β_5	$-1.2\,\mathrm{mV}$
β_6	$18\,\mathrm{mV}$
β_7	$10\,\mathrm{mV}$
β_8	$17.4\,\mathrm{mV}$

Parameter	Value
$C1$	$1\,\mu\mathrm{F/cm^2}$
$C2$	$1\,\mu\mathrm{F/cm^2}$
$C3$	$1\,\mu\mathrm{F/cm^2}$
$C4$	$1\,\mu\mathrm{F/cm^2}$
$C5$	$1\,\mu\mathrm{F/cm^2}$
$C6$	$1\,\mu\mathrm{F/cm^2}$
I_{app1}	$50\,\mu\mathrm{A/cm^2}$
I_{app2}	$50\,\mu\mathrm{A/cm^2}$
I_{app5}	$10\,\mu\mathrm{A/cm^2}$
I_{app6}	$10\,\mu\mathrm{A/cm^2}$

Table 1. Table of Parameters

are fast, and chemical connections happen at a slower pace. In the model there are three parameters controlling gap junction coupling on the soma, dendrites and axons, respectively. The dendrites are defined in a passive manner, whereas the somas and axons are excitable. Therefore, the axons and somas are able to create action potentials whereas the dendrites can only communicate it. The applied current on the axons is lower than on the somas.

Equations 7 describe gap junctions. It is important to note since we made a neuron with three compartments, then we need to add the connections between the compartments. The equations for the soma, are then described as follows:

$$C\frac{d}{dt}V_{s_i} = -g_{Ca}m_{inf}(V_{s_i})(V_{s_i}-V_{Ca}) - g_K w(V_{s_i}-V_K) - g_L(V_{s_i}-V_L) + I_{ext} \\ +g_{gs}(V_{s_j}-V_{s_i}) + g_{cd}\frac{(V_{d_i}-V_{s_i})}{1-p_d} + g_{ca}\frac{(V_{a_i}-V_{s_i})}{1-p_a} \tag{11}$$

Where g_{gs} is the gap junction coupling on the soma, g_c is the coupling for the neuron, and p_d and p_a are the so-called geometry parameters, which represent the relative size of the soma against the dendrite and axon, respectively. Therefore, the soma is connected to the dendrite and axon of the neuron, and to the soma of the other neuron through gap junctions.

The axon follows a similar equation, but in this case, it is not connected to the dendrites, only the soma:

$$C\frac{d}{dt}V_{axon_i} = -g_{Ca}m_{inf}(V_{axon_i})(V_{axon_i}-V_{Ca}) - g_K w(V_{axon_i}-V_K) - g_L(V_{axon_i}-V_L) + I_{ext} \\ +g_{gap_{axon}}(V_{axon_j}-V_{axon_i}) + g_{c_a}\frac{(V_{soma_i}-V_{axon_i})}{p_a} \tag{12}$$

And the dendrites have the following equations, as mentioned before, they are passive, so they do not create action potentials through ion changes.

$$C\frac{d}{dt}V_{dendrite_i} = -g_L(V_{dendrite_i}-V_L) + I_{ext} + g_{gap_{dendrite}}(V_{dendrite_j}-V_{dendrite_i}) + g_{c_d}\frac{(V_{soma_i}-V_{dendrite_i})}{p_d} \tag{13}$$

For the simulation it is possible to obtain both in-phase and anti-phase behaviour. This depends on the initial conditions. All values used in the simulation will be stated in the Appendix together with the code.

4.4 Simulation using Brian2

As seen above, the simulations in this project were done using Brian2. In the neuronal simulator, we used the built-in class called NeuronGroup to create the group of neurons. To be able to do that, it is necessary to specify certain parameters:

- The number of neurons in the group, N.
- The model of differential equations defining the group.
- The numerical integration method used for the model.

The differential equations used for the model were the ones mentioned beforehand (Equations 11, 12, 13). These can be written in Python indicating they are equations as shown in Listing 1.

```
1 eqs = '''
2 dV1/dt = (-g_Ca*minf1*(V1-V_Ca)-g_K*n1*(V1-V_K)-g_L*(V1-V_L)+Iapp_1
    +epsilon*(V2-V1)+g_c_d*(V3-V1)/(1-p_d)+g_c_a*(V5-V1)/(1-p_a))/C1
    : volt
```

```
3  dV2/dt = (-g_Ca*minf2*(V2-V_Ca)-g_K*n2*(V2-V_K)-g_L*(V2-V_L)+Iapp_2
       +epsilon*(V1-V2)+g_c_d*(V4-V2)/(1-p_d)+g_c_a*(V6-V2)/(1-p_a))/C2
       : volt
4  dV3/dt = (-g_L*(V3 - V_L) + g_gap_d*(V4 - V3)+g_c_d*(V1-V3)/p_d)/C3
       : volt
5  dV4/dt = (-g_L*(V4 - V_L) + g_gap_d*(V3 - V4)+g_c_d*(V2-V4)/p_d)/C4
       : volt
6  dV5/dt = (-g_Ca*minf5*(V5-V_Ca)-g_K*n5*(V5-V_K)-g_L*(V5 - V_L) +
       Iapp_5 + g_gap_a*(V6 - V5)+g_c_a*(V1-V5)/p_a)/C5 : volt
7  dV6/dt = (-g_Ca*minf6*(V6-V_Ca)-g_K*n6*(V6-V_K)-g_L*(V6 - V_L) +
       Iapp_6 + g_gap_a*(V5 - V6)+g_c_a*(V2-V6)/p_a)/C6 : volt
8  dn1/dt = (ninf1-n1)/taun1 : 1
9  dn2/dt = (ninf2-n2)/taun2 : 1
10 dn5/dt = (ninf5-n5)/taun5 : 1
11 dn6/dt = (ninf6-n6)/taun6 : 1
12 minf1 = 0.5*(1 + tanh((V1 - beta_1)/beta_2)) : 1
13 minf2 = 0.5*(1 + tanh((V2 - beta_1)/beta_2)) : 1
14 minf5 = 0.5*(1 + tanh((V5 - beta_1)/beta_2)) : 1
15 minf6 = 0.5*(1 + tanh((V6 - beta_1)/beta_2)) : 1
16 taun1 = (phi*cosh((V1 - beta_3)/(2*beta_4)))**-1 : second
17 taun2 = (phi*cosh((V2 - beta_3)/(2*beta_4)))**-1 : second
18 taun5 = (phi*cosh((V5 - beta_3)/(2*beta_4)))**-1 : second
19 taun6 = (phi*cosh((V6 - beta_3)/(2*beta_4)))**-1 : second
20 ninf1 = 0.5*(1 + tanh((V1 - beta_3)/beta_4)) : 1
21 ninf2 = 0.5*(1 + tanh((V2 - beta_3)/beta_4)) : 1
22 ninf5 = 0.5*(1 + tanh((V5 - beta_3)/beta_4)) : 1
23 ninf6 = 0.5*(1 + tanh((V6 - beta_3)/beta_4)) : 1
24 '''
```

Listing 1. Model Equations in Brian2

The definition of a NeuronGroup is done in the way indicated in Listing 2. In this research, we only used two coupled neuron, so $N = 2$. The equations defined in Listing 1 are used in the model by writing the specified name (in this case 'eqs') as the second term in the definition of the NeuronGroup.

```
1  neurons = NeuronGroup(N, eqs, method='exponential_euler')
```

Listing 2. Creation of a NeuronGroup using Brian2

Brian2 has some built in monitors that help with recording the necessary data. In this case, the function StateMonitor was used. This allows to record all the variables in the system of differential equations.

```
1      V1_monitor = StateMonitor(neurons, 'V1', record=True)
```

Listing 3. Creation of StateMonitor's in Brian2 example for variable V1

Once all this is set, the simulation can just be run with the 'run' function (Listing 4).

```
run(time*ms)
```

Listing 4. Command to run the simulation in Brian2

With Brian2 it is also possible to create spatial neurons with the class SpatialNeuron. However, if one wants to create connections between those neurons, it is much more efficient to use a NeuronGroup, since SpatialNeuron treats each neuron as an independent unit. For using SpatialNeuron we need to compile N amount of C++ files. In this case, we are only using two neurons, but in case this number increases, then we would have to compile many files representing the computations updating the neurons. Furthermore, for using SpatialNeuron, every pair of neurons needs to be connected through Synapses.

5 RESULTS AND DISCUSSION

In the previous section the Morris-Lecar model was considered (Morris and Lecar, 1981). The neuronal connections between neurons composed of a dendrite, an axon, and a soma were described (Equations 11, 12, 13). In this section the impact on synchronization of adding the aforementioned compartments to the neuron will be studied systematically by the progressive change of several parameters.

To get a better understanding of the model, the focus was on the smallest possible network, composed by only two neurons. The initial goal was to be able to reproduce both In-Phase and Anti-Phase behaviour. For this, two point-neurons with gap junction coupling were used. All the parameters for the model also had the same value, the only differences were they initial conditions used. If one wants to simulate In-Phase behaviours then the initial values should be $X_0 = [40, 0.04, 40, 0.074]$, for Anti-Phase behaviour the values should be $X_0 = [40, 0.04, -40, 0.074]$. The simulation of both behaviours can be seen in Figure 8.

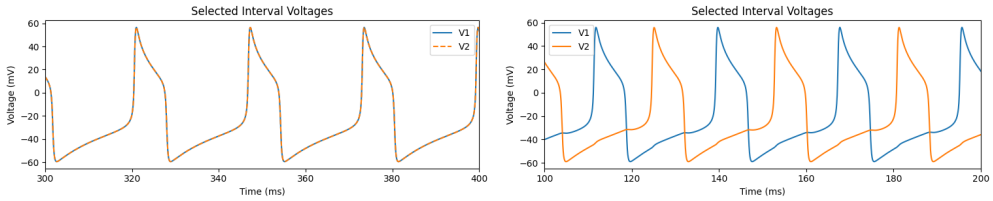

Figure 8. In and Anti phase behaviours obtained using the initial conditions mentioned above. The parameters are $\varepsilon = 0.1$, $g_c = 0.001$, $g_{pa} = g_{pd} = 0.1$. What differs are the initial conditions, In-Phase: $X_0 = [40, 0.04, 40, 0.074]$, Anti-Phase: $X_0 = [40, 0.04, -40, 0.074]$.

For each simulation, six different graphs were plotted. These represented:

- Changes in Soma voltages over time for both neurons.
- Selected interval of the changes in Soma voltages over time for both neurons.
- Changes in Dendrite voltages over time for both neurons.

- Changes in Axon voltages over time for both neurons.
- Composed signal obtained from the addition of the voltages of both neurons over time.
- Periodogram.

Then a systematic study was conducted to determine the effect changes in different parameters have in synchronization over time. The parameters that were:

- Coupling between soma-dendrite (0.001-0.1).
- Coupling between soma-axon (0.001-0.1).
- Gap junction coupling between somas (0.001-0.1).
- Gap junction coupling between dendrites (0.001-0.1).
- Gap junction coupling between axons 0.001-0.1).
- Relative size soma-dendrite and soma-axon (0.01-0.1).

The main goal was to see if, and how adding compartments to the neuron changed its long time behaviour, and how gap junctions destroy Anti-Phase Synchrony. To study this behaviour the main graph used was the composed signal one. The reasoning behind this is that it is easier to study behaviour long term. Here, we see three different types of behaviours. First of all, for strong enough coupling between the neurons, the dynamics become mutually synchronized. When we have this case, then at some point the composed signals grows until reaching 100mV. In case the parameter C, which corresponds to the cell's membrane capacitance, is different for both neurons, sometimes we encounter the behaviour of Figure 9c. Where the neurons become In-Phase for one spike, then they go back to Anti-Phase behaviour, to then return to being In-Phase for one spike, and so on. The last case happens when coupling is not strong enough, and then the neurons do not synchronize. This is seen in the composed signal graph since the behaviour stays the same and the voltage does not go above 20mV.

For being able to compare the different long term behaviours the value where the composed signal starts to increase at a fast rate was recorded. The exact value taken is the start of the last spike where the second peak is smaller than the first one (see Figure 10).

The gap junctions were placed at the soma, the dendrite, and the axon separately, and then the long-term behaviour was recorded in a table.

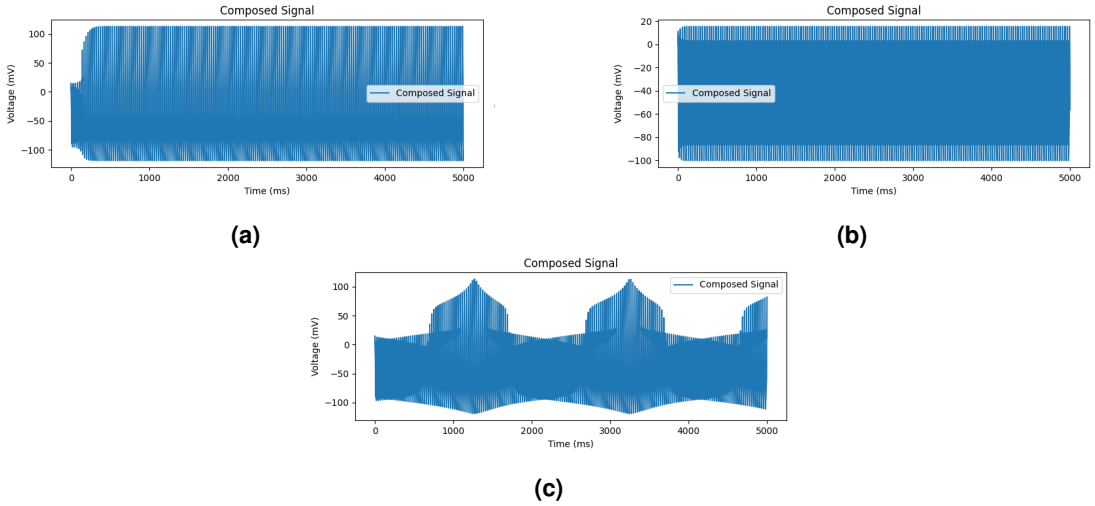

Figure 9. Three different observed long time behaviours of (a)synchronization. Graph a represents In-Phase synchronization. The values used are gap junction coupling $\varepsilon = 0.005$. In graph b one can see Anti-Phase behaviour, the values used were a gap junction coupling on the soma of $\varepsilon = 0.05$ and a coupling of $g_c = 0.05$. For c, gap junction coupling between axons is $g_{c_a} = 0.01$ and coupling $g_c = 0.001$.

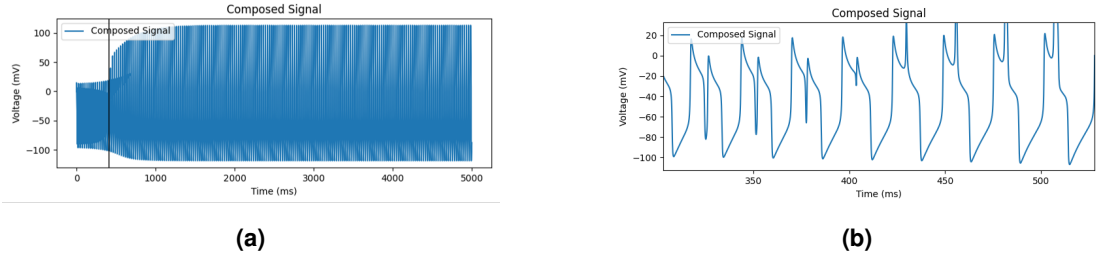

Figure 10. Point recorded for the comparison table (Table 1).

5.1 Gap Junction Coupling placed at the Soma

In this section we dive deeper into the long-term behaviour of the system when the gap junction coupling is placed at the soma, and how the behaviour varies depending on the values used.

g_c	Gap coupling soma (ε)				
	0.001	0.005	0.010	0.050	0.100
0.000	3976	779	386	101	8
0.001	4166	835	413	128.5	22
0.005	5090.5	1030	522	A	A
0.010	7020	1512.5	848.5	A	A
0.050	A	A	A	A	8
0.100	A	A	A	A	5

Table 2. Geometry parameter fixed at $g_p = 0.1$.

g_c	Gap coupling soma (ε)				
	0.001	0.005	0.010	0.050	0.100
0.000	3976	779	386	101	8
0.001	4139.5	832.5	413	128.5	22
0.005	4982	1023	522	A	A
0.010	6504.5	1377	740.5	A	A
0.050	A	A	A	A	8
0.100	A	A	A	A	8

Table 3. Geometry parameter fixed at $g_p = 0.05$.

g_c	Gap coupling soma (ε)				
	0.001	0.005	0.010	0.050	0.100
0.000	3976	779	386	101	8
0.001	4139	832.5	413	128.5	22
0.005	4767	969	495	A	A
0.010	5448	1106	577	A	A
0.050	4767	1819	1124.5	A	69
0.100	4112.5	2070.5	1247.5	A	38

Table 4. Geometry parameter fixed at $g_p = 0.01$.

Table 5. Table obtained by recording the Composed Signal point mentioned in Figure 10 when using different coupling intensities. If the system reaches In-Phase behaviour, the aforementioned point recorded is the time in ms seen at the table. When the system maintains Anti-Phase behaviour the value is set to "A". Time in ms and gap junction coupling in mS/cm^2.

5.1.1 Point vs Multi-Compartment Neuron

For this thesis, a simulation including dendrites and axons was set up. In Tables 2, 3, and 4 the results can be seen. First of all, it is important to note the difference between the first row of results (row 3) and the rest. The first row has coupling $g_c = 0.0$, which means that there is no coupling between the soma and the axon, and the soma and the dendrites. Therefore, the simulation treats the system as a point-neuron, only considering the cell body. These values are the same in each table, which is a confirmation that the simulation works. If the morphology would not affect the

behaviour of the system, then these values would remain constant for the rest of the rows. Nevertheless, that is not the case, which confirms that neuronal morphology does have an impact on the network synchronization.

To further analyse the results the tables were looked at in two different directions. First, one could fix a value for coupling (first column) and analyse how the long term behaviour of the system varies with increasing gap junction values on the soma, axon, and dendrites, respectively. It can also be done the other way around, by fixing the value of the gap junction coupling, and varying the coupling between the same neuron, and seeing the effects of this. This is what is done in the following sections.

5.1.2 Fixed Neuron Coupling

In this section we will analyse the behaviour when there is fixed coupling between soma, dendrite, or axon of the same neuron. The results are analysed looking at the gap junctions separately.

With a fixed coupling value, by increasing gap junction coupling at the soma, one can observe how the neuron starts to reach In-Phase synchrony faster. Therefore, the neuron takes less time to reach synchrony. The evolution can also be plotted. In that case we obtain Figure 11. In this figure, the plotted lines are descending, which represents how the network reaches In-Phase behaviour faster with an increase of the coupling strength.

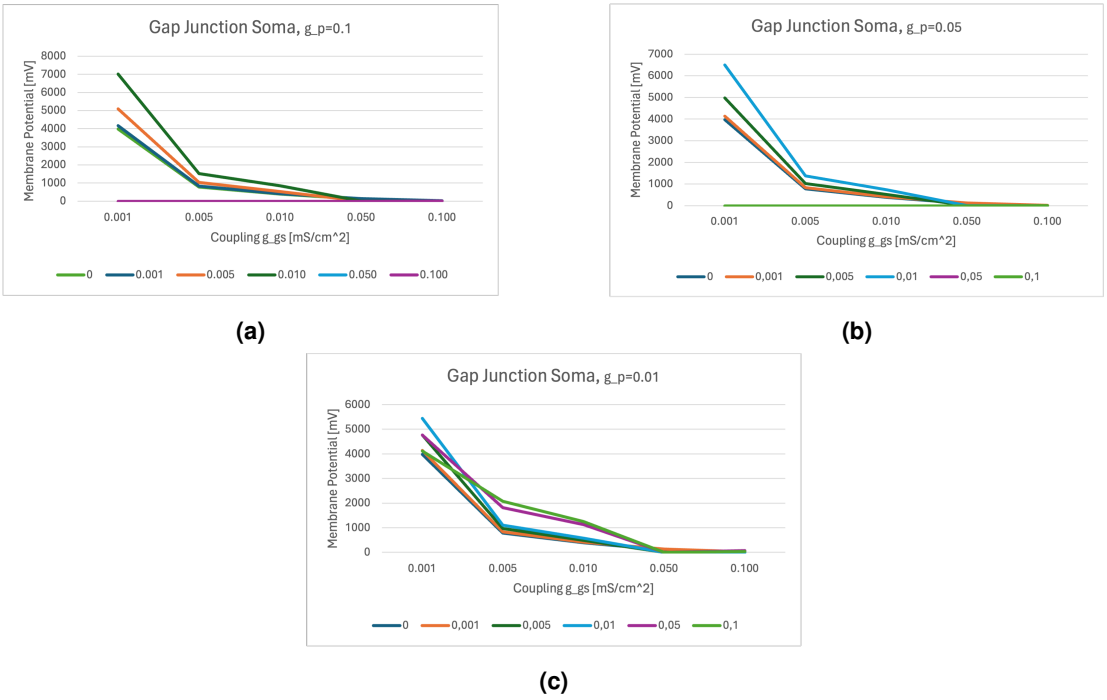

Figure 11. Plotting of the values from Tables 2, 3, and 4 with a fixed g_c, and different values for the geometry parameter g_c mentioned in the Title of each graph.

The behaviour when the geometry parameter is $g_p = 0.1$ resembles the one of $g_p = 0.05$. When the geometry parameter is smaller, $g_p = 0.01$, then we observe a slightly different behaviour. In this case the system still reaches In-Phase behaviour when the coupling

is $g_c = 0.05$ or $g_c = 0.1$, which does not happen for the other values. This is represented with the plotted lines $g_c = 0.05$ and $g_c = 0.1$ (green and purple). Aside from those two lines, the network would still resemble the behaviours with the other geometry parameter ($g_p = 0.1$ or $g_p = 0.05$).

Additionally, as the gap junction coupling increases, the system takes less time to reach In-Phase synchrony. The start of the synchronization process keeps getting closer to 0, until the system stops reaching synchrony altogether.

When the geometry parameter is smaller, the network takes less time to synchronize. This is more noticeable with stronger coupling, since with weak coupling the results obtained are extremely similar, with little to no noticeable change at all.

5.1.3 Fixed Gap Junction Coupling

In this case, the fixed value is the Gap Junction Coupling at the soma.

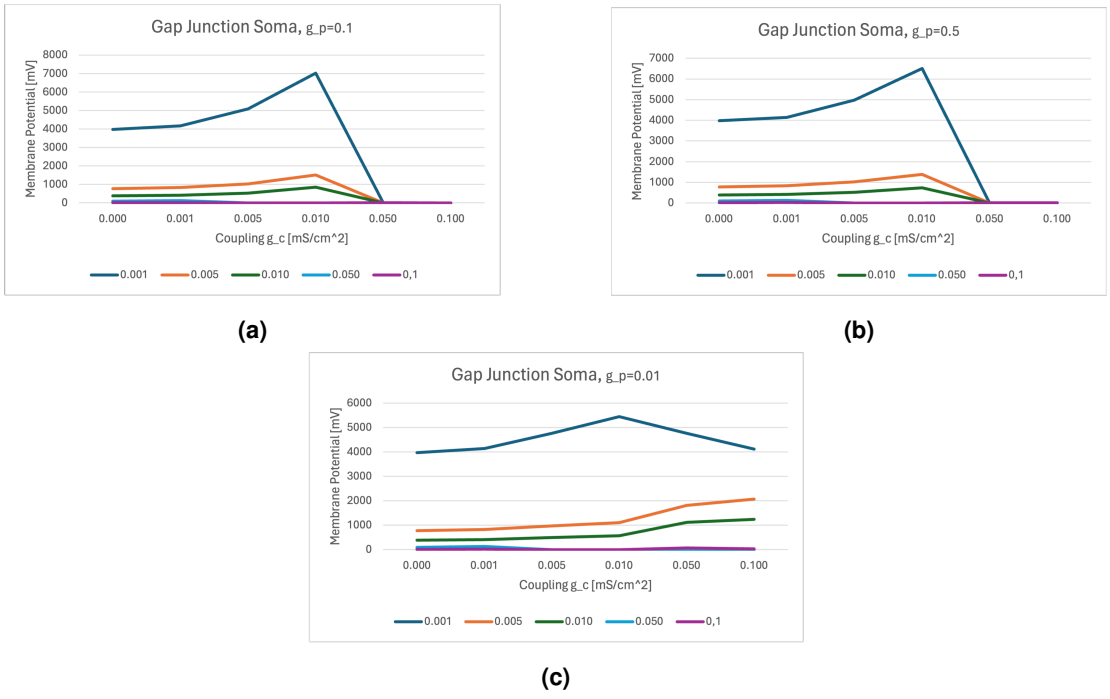

Figure 12. Plotting of the values from Tables 2, 3, and 4 with a fixed ε, and different values for the geometry parameter g_c mentioned in the Title of each graph.

Again, one can see how the graphs for which the geometry parameter is $g_p = 0.1$ and $g_p = 0.05$ resemble each other. In this case, the system takes the longest to synchronise when the coupling is $g_c = 0.01$. For stronger coupling, the system fails to reach In-Phase synchrony in most cases. It still seems to perform its best at synchronising when the geometry parameter is smaller ($g_p = 0.01$). With this, it is meant that it reaches synchrony at more instances, and in most cases faster. Another thing that can be observed is how the long-term behaviour varies less when the gap junction coupling on the soma is $\varepsilon = 0.005$ or $\varepsilon = 0.010$. This can be observed in Figure 12 represented by flatter lines.

5.2 Gap Junction Coupling placed at the Axon

Axons are also excitatory compartments, like somas. Therefore, every time the soma spikes, the axon will generate an action potential. Axons generating action potentials can lead to synchronized firing of neurons. Additionally, axonal gap junctions can generate VFOs and play a role in generating ripple oscillations (Traub et al., 2002).

Comparing the amount of times the network reaches synchrony when we place the gap junction coupling at the axons, with when we place it at the soma, we see that the system is more unstable in this case. For most of the simulations runs, the system fails to synchronise. We can only observe synchrony when gap junction coupling is strong enough ($g_{gap_a} \geq 0.05$).

When comparing the three tables (Table 6, 7, and 8) with each other, one can observe how again, the system synchronises the most when the geometry parameter is the smallest.

In this case, in Table 8, when the parameters taken are $g_c = 0.010$ and $g_{gap_a} = 0.100$ respectively, we obtained a different type of long-term behaviour. In this case, there is a phase-shift. The system starts in Anti-Phase synchrony, and then the phases shift so that the spikes happen.

Furthermore, when the coupling is sufficiently strong ($g_c = 0.1$) then the system maintains the Anti-Phase behaviour if the geometry parameter is $g_p = 0.1$ or $g_p = 0.05$, and it case it does not synchronise. This is represented in Table 9 by an "A". In the other cases, there is no Anti-Phase behaviour, instead, there seems to be an slight phase shift. There is one case, marked with a "*", where there seems to be transient phase-locking (Figure 13).

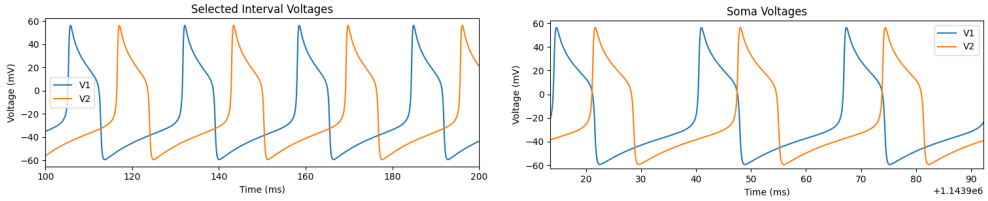

Figure 13. Phase shift when $g_c = 0.010$ and $g_{gap_a} = 0.100$. On the left is represented the initial state, and on the right the state after the shift.

g_c	Gap coupling axon (g_{gap_a})				
	0.001	0.005	0.010	0.050	0.100
0.000	X	X	X	X	X
0.001	X	X	X	X	X
0.005	X	X	X	X	X
0.010	X	X	X	X	X
0.050	X	X	18315.5	3874	4831,1
0.100	A	A	A	A	A

Table 6. Geometry parameter fixed at $g_p = 0.1$.

g_c	Gap coupling axon (g_{gap_a})				
	0.001	0.005	0.010	0.050	0.100
0.000	X	X	X	X	X
0.001	X	X	X	X	X
0.005	X	X	X	X	X
0.010	X	X	X	X	X
0.050	X	X	X	14348.5	8466
0.100	A	A	A	A	A

Table 7. Geometry parameter fixed at $g_p = 0.05$.

g_c	Gap coupling axon (g_{gap_a})				
	0.001	0.005	0.010	0.050	0.100
0.000	X	X	X	X	X
0.001	X	X	X	X	X
0.005	X	X	X	14736.5	*
0.010	X	X	X	16328	8437.5
0.050	X	X	X	13830	6932
0.100	X	X	X	13207.5	6694.5

Table 8. Geometry parameter fixed at $g_p = 0.01$.

Table 9. Table obtained by recording the Composed Signal point mentioned in Figure 10 when using different coupling intensities. If the system did not synchronise then it is filled with an "X", and if the system did not synchronize but it exhibited Anti-Phase behaviour then it is filled with an "A". Time in ms and gap junction coupling in mS/cm^2.

5.3 Gap Junction place at the dendrites

The network is the most unstable when the gap junctions are placed at the dendrites. But the behaviour is similar to the one obtained for the axons.

g_c	Gap coupling dendrite (g_{gap_d})				
	0.001	0.005	0.010	0.050	0.100
0.000	X	X	X	X	X
0.001	X	X	X	X	X
0.005	X	X	X	X	X
0.010	X	X	X	X	110293
0.050	X	X	X	X	22765
0.100	A	A	A	A	A

Table 10. Geometry parameter fixed at $g_p = 0.1$.

g_c	Gap coupling dendrite (g_{gap_d})				
	0.001	0.005	0.010	0.050	0.100
0.000	X	X	X	X	X
0.001	X	X	X	X	X
0.005	X	X	X	X	X
0.010	X	X	X	X	X
0.050	X	X	X	X	12067.5
0.100	A	A	A	A	A

Table 11. Geometry parameter fixed at $g_p = 0.05$.

g_c	Gap coupling dendrite (g_{gap_d})				
	0.001	0.005	0.010	0.050	0.100
0.000	X	X	X	X	X
0.001	X	X	X	X	X
0.005	X	X	X	X	X
0.010	X	X	X	48738.5	25250.5
0.050	X	X	X	16415	8324
0.100	X	X	X	14497.5	7312.5

Table 12. Geometry parameter fixed at $g_P = 0.01$.

Table 13. Table obtained by recording the Composed Signal point mentioned in Figure 10 when using different coupling intensities. If the system did not synchronise then it is filled with an "X", and if the system did not synchronize but it exhibited Anti-Phase behaviour then it is filled with an "A". Time in ms and gap junction coupling in mS/cm^2.

Additionally, differently to when the gap junctions were only placed at the soma, when the gap junctions are placed at the dendrites there is only Anti-Phase behaviour when the coupling is strong enough $g_c = 0.1$. For all the other cases, the spikes are not in synchrony. Except for the cases indicated in Table 13 (when $g_c = 0.05$ and $g_c d = 0.1$, which reaches IPS). The behaviour when the system does not synchronise and is also not Anti-Phase can be seen in Figure 14.

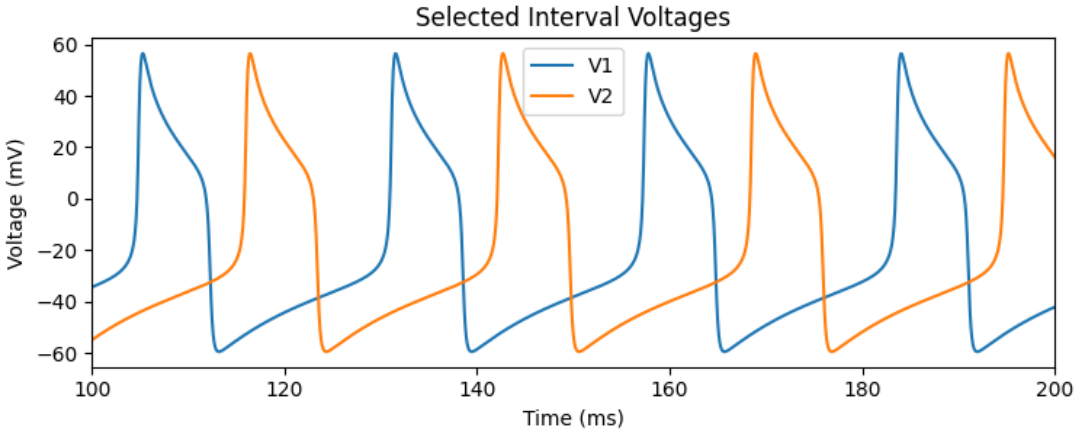

Figure 14. In this image the potentials of the soma are plotted when there is a gap junction placed at the dendrite of $g_{cd} = 0.001$, coupling $g_c = 0.001$, and geometry parameter $g_p = 0.1$.

5.4 Relation to epilepsy

The previous sections have analysed the long-term behaviour of the system. Mainly if the network was able to reach synchronization or not. If a neuronal network bursts highly synchronized action potentials there could be depolarizing phase shifts. These are associated with the initiation of seizures (Jiruska et al., 2013). Furthermore, electrical coupling, like the one used for the simulation, can also facilitate synchronous firing.

Aside from the synchronization to be dangerous for the initiation of seizures, it can also propagate them. This happens when additional networks are recruited by the synchronized network (Přibylová et al., 2024). If this happens, the seizure could expand to other parts of the brain.

5.5 Discussion of Results

Several articles (Caire et al., 2020; Gernster et al., 2014) affirmed that the synchronization behaviour of a system is altered by biophysically realistic modelling of the morphology of a neuron. This can be seen mainly when the gap junctions are placed at the soma. From Table 5 and Figure 12 one can see how the time it takes for the system to reach In-Phase synchrony varies depending on the strength of g_c. Otherwise, the system maintains Anti-Phase behaviour.

When the gap junctions were placed at the axons or dendrites, in most cases the Anti-Phase behaviour was destroyed. With strong coupling the simulation was able to maintain the Anti-Phase synchrony, and in some cases it reached In-Phase synchrony. Previous research has affirmed that neuronal morphology has an impact on neuronal synchronization. Gowers and Schreiber (2024) constructed a model with an excitatory soma and a passive dendrite. It was observed how adding the dendrite can switch the behaviour from synchronous to asynchronous. Which corresponds to the observations made in this thesis.

Zeng et al. (2007) showed how axonal synchronizations is more present with increased coupling strength, which is also supported by our findings.

6 CONCLUSION

This project used the Morris-Lecar model to analyse the synchronization of a multi-compartment neuronal network. The network was connected through gap junction coupling, with gap junctions placed at the soma, axon, and dendrites. Overall, the research examined how neuronal morphology and coupling parameters can influence the overall synchronization of a neuronal network.

The findings revealed that the system reaches IPS at different velocities when the compartments are added to the simulation. Which reinforces previous research stating the influence of adding neuronal morphology to the simulation. In the cases where the network reached synchrony, stronger coupling parameters were found to be more effective. In these cases, the system reached synchrony faster.

When the gap junctions were placed at the soma, the simulation always either maintained the APS or switched to IPS. When the gap junctions were placed at the axon or the dendrite, synchronous behaviour was only found for strong coupling.

7 ACKNOWLEDGEMENTS

I would like to thank my daily supervisor, Dr. Hil Meijer, for all the extremely useful meetings, and all the help offered in the process of completing this research. Additionally, for introducing me to the field of computational neuroscience and some of its potential applications. Furthermore, I would like to thank my ATLAS supervisor, Dr. José Alfredo Álvarez Chávez, for helping throughout the process. Last but not least, I would like to thank my family and friends for providing support throughout this experience.

REFERENCES

Bragin, A., Wilson, C. D., and Engel, J. P. (2000). Chronic epileptogenesis requires development of a network of pathologically interconnected neuron clusters: A hypothesis. *Epilepsia*, 41:S144–S152.

Brown, P. (2003). Oscillatory nature of human basal ganglia activity: Relationship to the pathophysiology of parkinson's disease. *Movement Disorders*, 18:357–363.

Brázdil, M., Worrell, G. A., Trávníček, V., Pail, M., Roman, R., Plešinger, F., Klimeš, P., Cimbálník, J., Stacey, W., and Jurák, P. (2023). Ultra fast oscillations in the human brain and their functional significance. *medRxiv (Cold Spring Harbor Laboratory)*.

Cai, Z., Sohrabpour, A., Jiang, H., Ye, S., Joseph, B., Brinkmann, B. H., Worrell, G. A., and He, B. (2021). Noninvasive high-frequency oscillations riding spikes delineates epileptogenic sources. *Proceedings of the National Academy of Sciences*, 118.

Caire, M. J., Reddy, V., and Varacallo, M. (2020). *Physiology, Synapse*. StatPearls Publishing.

Cymerblit-Sabba, A. and Schiller, Y. (2012). Development of hypersynchrony in the cortical network during chemoconvulsant-induced epileptic seizures in vivo. *Journal of Neurophysiology*, 107:1718–1730.

Engel, J. and da Silva, F. L. (2012). High-frequency oscillations – where we are and where we need to go. *Progress in Neurobiology*, 98:316–318.

Fedele, T., Burnos, S., Boran, E., Krayenbühl, N., Hilfiker, P., Grunwald, T., and Sarnthein, J. (2017). Resection of high frequency oscillations predicts seizure outcome in the individual patient. *Scientific Reports*, 7.

Foffani, G., Uzcategui, Y. G., Gal, B., and Menendez de la Prida, L. (2007). Reduced spike-timing reliability correlates with the emergence of fast ripples in the rat epileptic hippocampus. *Neuron*, 55.

Gernster, W., Kistler, W. M., Naud, R., and Paninski, L. (2014). *Neuronal Dynamics*. Cambridge University Press.

Gowers, R. P. and Schreiber, S. (2024). How neuronal morphology impacts the synchronisation state of neuronal networks. *PLOS Computational Biology*, 20:e1011874.

Hodgkin, A. L. and Huxley, A. F. (1952). A quantitative description of membrane current and its application to conduction and excitation in nerve. *The Journal of Physiology*, 117:500–544.

Jefferys, J. G., Menendez de la Prida, L., Wendling, F., Bragin, A., Avoli, M., Timofeev, I., and Lopes da Silva, F. H. (2012). Mechanisms of physiological and epileptic hfo generation. *Progress in Neurobiology*, 98:250–264.

Jiruska, P., de Curtis, M., Jefferys, J. G. R., Schevon, C. A., Schiff, S. J., and Schindler, K. (2013). Synchronization and desynchronization in epilepsy: controversies and hypotheses. *The Journal of Physiology*, 591:787–797.

Kandel, E. R., Schwartz, J. H., Jessell, T. M., Siegelbaum, S. A., and Hudspeth, A. (2013). *Principles Of Neural Science*. Elsevier.

Kazemi, S. and Jamali, Y. (2022). Phase synchronization and measure of criticality in a network of neural mass models. *Scientific Reports*, 12:1319.

Morris, C. and Lecar, H. (1981). Voltage oscillations in the barnacle giant muscle fiber. *Biophysical Journal*, 35:193–213.

NHS (2020). Treatment - epilepsy. Accessed: 2024-06-01.

Ofer, N., Shefi, O., and Yaari, G. (2017). Branching morphology determines signal propagation dynamics in neurons. *Scientific Reports*, 7.

Panzica, F., Varotto, G., Rotondi, F., Spreafico, R., and Franceschetti, S. (2013). Identification of the epileptogenic zone from stereo-eeg signals: A connectivity-graph theory approach. *Frontiers in Neurology*, 4.

Přibylová, L., Ševčík, J., Eclerová, V., Klimeš, P., Brázdil, M., and Meijer, H. (2024). Weak coupling of neurons enables very high-frequency and ultra-fast oscillations through the interplay of synchronized phase-shifts. *Network neuroscience*, 8:293–318.

Ratté, S., Hong, S., De Schutter, E., and Prescott, S. (2013). Impact of neuronal properties on network coding: Roles of spike initiation dynamics and robust synchrony transfer. *ResearchGate*.

Traub, R. D., Draguhn, A., Whittington, M. A., Baldeweg, T., Bibbig, A., Buhl, E. , and Schmitz, D. (2002). Axonal gap junctions between principal neurons: A novel source of network oscillations, and perhaps epileptogenesis. *Reviews in the Neurosciences*, 13:1–30.

Tsumoto, K., Kitajima, H., Yoshinaga, T., Aihara, K., and Kawakami, H. (2006). Bifurcations in morris-lecar neuron model. *Elsevier*, 69.

Tülay, E. E., Güntekin, B., Yener, G., Bayram, A., Başar-Eroğlu, C., and Demiralp, T.

(2020). Evoked and induced eeg oscillations to visual targets reveal a differential pattern of change along the spectrum of cognitive decline in alzheimer's disease. *International Journal of Psychophysiology*, 155:41–48.

van Pelt, J., van Ooyen, A., and Uylings, H. B. M. (2001). The need for integrating neuronal morphology databases and computational environments in exploring neuronal structure and function. *Anatomy and Embryology*, 204:255–265.

van Putten, M. J. (2020). *Dynamics of Neural Networks*. Springer Berlin, Heidelberg.

van Wijk, B. C. M., Beek, P. J., and Daffertshofer, A. (2012). Neural synchrony within the motor system: what have we learned so far? *Frontiers in Human Neuroscience*, 6.

Zeng, S., Tang, Y., and Jung, P. (2007). Spiking synchronization of ion channel clusters on an axon. *Physical review. E, Statistical, nonlinear and soft matter physics*, 76.

Zijlmans, M., Jiruska, P., Zelmann, R., Leijten, F. S., Jefferys, J. G., and Gotman, J. (2012). High-frequency oscillations as a new biomarker in epilepsy. *Annals of Neurology*, 71:169–178.

Zweiphenning, W. J. E. M., , v., E.C, N., Frans, Ferrier, C. H., Gebbink, T., Huiskamp, G., , M., , M., Bourez, M., Goemans, S. A. M., Straumann, S., , P., Gosselaar, P. H., van Eijsden, P., Otte, W. M., van Diessen, E., Braun, K. P., Zijlmans, M., Bloemen-Carlier, E. M., Cibulková, V., de Munnink, R., , S., Eijkemans, M., Ophorst-van, J. M., Velders, A., J.J, C., Zwemmer, J., , R., Smeding, H., , L., de Bresser, J., de, A., and Dankbaar, J.-W. (2022). Intraoperative electrocorticography using high-frequency oscillations or spikes to tailor epilepsy surgery in the netherlands (the hfo trial): a randomised, single-blind, adaptive non-inferiority trial. *The Lancet*, 21:982–993.

8 APPENDIX

8.1 Full code

```
1
2
3  from brian2 import *
4
5  # ----------------------------------------------------------------
       Parameters
       ----------------------------------------------------------------
6  g_Ca = 4*mS/cm**2
7  g_K = 8*mS/cm**2
8  g_L = 2*mS/cm**2
9  V_Ca = 120*mV
10 V_K = -80*mV
11 V_L = -60*mV
12 phi = 1/(15.0*ms)
13 beta_1 = -1.2*mV
14 beta_2 = 18*mV
15 beta_3 = 10*mV
16 beta_4 = 17.4*mV
17 beta_5 = -1.2*mV
18 beta_6 = 18*mV
19 beta_7 = 10*mV
20 beta_8 = 17.4*mV
21 C1 = 1*uF/cm**2
22 C2 = 1*uF/cm**2
23 C3 = 1*uF/cm**2
24 C4 = 1*uF/cm**2
25 C5 = 1*uF/cm**2
26 C6 = 1*uF/cm**2
27 Iapp_1 = 50*uA/cm**2
28 Iapp_2 = 50*uA/cm**2
29 Iapp_5 = 10*uA/cm**2
30 Iapp_6 = 10*uA/cm**2
31 epsilon = 0.01 * mS/cm**2 # This is gap-junction coupling on the soma
32 g_gap_a = 0.0*mS/cm**2
33 g_gap_d = 0.0*mS/cm**2
34 g_c_d = 0.001*mS/cm**2 # Coupling Soma-Dendrite
35 g_c_a = g_c_d # Coupling Soma-Axon rn set to the same as dendrite
36 p_d = 0.05 # geometry parameter (relative size of soma vs dendrite)
37 p_a = p_d # geometry parameter (relative size of soma vs axon)
38
```

```
# ------------------------------------------------------------
    Morphology
    ------------------------------------------------------------

# Same morphology for both neurons
#morpho = Soma(30*um)
#morpho.axon = Cylinder(diameter=1*um, length=300*um, n=1)
#morpho.dendrite = Cylinder(diameter=1*um, length=100*um, n=1)

gL = 0.002*siemens/cm**2
EL = -60*mV

# ------------------------------------------------------------
    Model
    ------------------------------------------------------------

eqs = '''
dV1/dt = (-g_Ca*minf1*(V1-V_Ca)-g_K*n1*(V1-V_K)-g_L*(V1-V_L)+Iapp_1
    +epsilon*(V2-V1)+g_c_d*(V3-V1)/(1-p_d)+g_c_a*(V5-V1)/(1-p_a))/C1
    : volt
dV2/dt = (-g_Ca*minf2*(V2-V_Ca)-g_K*n2*(V2-V_K)-g_L*(V2-V_L)+Iapp_2
    +epsilon*(V1-V2)+g_c_d*(V4-V2)/(1-p_d)+g_c_a*(V6-V2)/(1-p_a))/C2
    : volt
dV3/dt = (-g_L*(V3 - V_L) + g_gap_d*(V4 - V3)+g_c_d*(V1-V3)/p_d)/C3
    : volt
dV4/dt = (-g_L*(V4 - V_L) + g_gap_d*(V3 - V4)+g_c_d*(V2-V4)/p_d)/C4
    : volt
dV5/dt = (-g_Ca*minf5*(V5-V_Ca)-g_K*n5*(V5-V_K)-g_L*(V5 - V_L) +
    Iapp_5 + g_gap_a*(V6 - V5)+g_c_a*(V1-V5)/p_a)/C5 : volt
dV6/dt = (-g_Ca*minf6*(V6-V_Ca)-g_K*n6*(V6-V_K)-g_L*(V6 - V_L) +
    Iapp_6 + g_gap_a*(V5 - V6)+g_c_a*(V2-V6)/p_a)/C6 : volt
dn1/dt = (ninf1-n1)/taun1 : 1
dn2/dt = (ninf2-n2)/taun2 : 1
dn5/dt = (ninf5-n5)/taun5 : 1
dn6/dt = (ninf6-n6)/taun6 : 1
minf1 = 0.5*(1 + tanh((V1 - beta_1)/beta_2)) : 1
minf2 = 0.5*(1 + tanh((V2 - beta_1)/beta_2)) : 1
minf5 = 0.5*(1 + tanh((V5 - beta_1)/beta_2)) : 1
minf6 = 0.5*(1 + tanh((V6 - beta_1)/beta_2)) : 1
taun1 = (phi*cosh((V1 - beta_3)/(2*beta_4)))**-1 : second
taun2 = (phi*cosh((V2 - beta_3)/(2*beta_4)))**-1 : second
taun5 = (phi*cosh((V5 - beta_3)/(2*beta_4)))**-1 : second
taun6 = (phi*cosh((V6 - beta_3)/(2*beta_4)))**-1 : second
ninf1 = 0.5*(1 + tanh((V1 - beta_3)/beta_4)) : 1
```

```
ninf2 = 0.5*(1 + tanh((V2 - beta_3)/beta_4)) : 1
ninf5 = 0.5*(1 + tanh((V5 - beta_3)/beta_4)) : 1
ninf6 = 0.5*(1 + tanh((V6 - beta_3)/beta_4)) : 1
'''

# ------------------------------------------------------------
    Creation neurons
    ------------------------------------------------------------

# Neuron Group
N = 1
neurons = NeuronGroup(N, eqs, method='exponential_euler')

# Somas
neurons.V1 = 40*mV
neurons.n1 = 0.04
neurons.V2 = -40*mV
neurons.n2 = 0.074

# Dendrites
neurons.V3 = -60*mV
neurons.V4 = -60*mV

# Axons
neurons.V5 = 60*mV
neurons.n5 = 0.06
neurons.V6 = -60*mV
neurons.n6 = 0.06


# ------------------------------------------------------------
    Monitors
    ------------------------------------------------------------
V1_monitor = StateMonitor(neurons, 'V1', record=True)
V2_monitor = StateMonitor(neurons, 'V2', record=True)
V3_monitor = StateMonitor(neurons, 'V3', record=True)
V4_monitor = StateMonitor(neurons, 'V4', record=True)
V5_monitor = StateMonitor(neurons, 'V5', record=True)
V6_monitor = StateMonitor(neurons, 'V6', record=True)
n1_monitor = StateMonitor(neurons, 'n1', record=True)
n2_monitor = StateMonitor(neurons, 'n2', record=True)

# ------------------------------------------------------------
    Simulation
```

```
    ------------------------------------------------------------

run(840 * ms)

print("SIM DONE")

# ------------------------------------------------------------
    Plotting
    ------------------------------------------------------------
fig, axs = plt.subplots(3, 2, figsize=(15, 10))
axs[0, 0].plot(V1_monitor.t/ms, V1_monitor.V1[0]/mV,label='V1')
axs[0, 0].plot(V2_monitor.t/ms, V2_monitor.V2[0]/mV,  label='V2')
axs[0, 0].set(xlabel='Time (ms)', ylabel='Voltage (mV)', title='Soma
    Voltages')
axs[0, 0].legend()

axs[0, 1].plot(V3_monitor.t/ms, V3_monitor.V3[0]/mV, label='V3')
axs[0, 1].plot(V4_monitor.t/ms, V4_monitor.V4[0]/mV, label='V4')
axs[0, 1].set(ylim=(-70,-50), xlabel='Time (ms)', ylabel='Voltage
    (mV)', title='Dendrite Voltages')
axs[0, 1].legend()

axs[1, 0].plot(V1_monitor.t/ms, V1_monitor.V1[0]/mV, label='V1')
axs[1, 0].plot(V2_monitor.t/ms, V2_monitor.V2[0]/mV, label='V2')
axs[1, 0].set(xlabel='Time (ms)', ylabel='Voltage (mV)',
    title='Selected Interval Voltages')
axs[1, 0].set_xlim([100, 200])
axs[1, 0].legend()

axs[1, 1].plot(V5_monitor.t/ms, V5_monitor.V5[0]/mV, label='V5')
axs[1, 1].plot(V6_monitor.t/ms, V6_monitor.V6[0]/mV, label='V6')
axs[1, 1].set(xlabel='Time (ms)', ylabel='Voltage (mV)', title='Axon
    Voltages')
axs[1, 1].legend()

composed_signal = V1_monitor.V1[0] + V2_monitor.V2[0]
axs[2, 0].plot(V1_monitor.t/ms, composed_signal/mV, label='Composed
    Signal')
axs[2, 0].set(xlabel='Time (ms)', ylabel='Voltage (mV)',
    title='Composed Signal')
axs[2, 0].legend()

# Compute periodograms
from scipy.signal import periodogram
```

```
145
146 def compute_periodogram(signal, dt):
147     f, Pxx = periodogram(signal, 1/dt)
148     return f, Pxx
149
150 f1, Pxx1 = compute_periodogram(V1_monitor.V1[0], defaultclock.dt)
151 f2, Pxx2 = compute_periodogram(V2_monitor.V2[0], defaultclock.dt)
152
153 axs[2, 1].plot(f1, Pxx1, label='V1 Periodogram')
154 axs[2, 1].plot(f2, Pxx2, label='V2 Periodogram')
155 axs[2, 1].set(xlabel='Frequency (Hz)', ylabel='Power',
       title='Periodograms')
156 axs[2, 1].legend()
157
158 plt.tight_layout()
159 plt.show()
```

Listing 5. Model Equations in Brian2